Cross-neutralizing antibodies bind a SARS-CoV-2 cryptic site and resist to circulating variants

Tingting Li
State Key Laboratory of Molecular Vaccinology and Molecular Diagnostics, School of Life Sciences, Xiamen University

Wenhui Xue
State Key Laboratory of Molecular Vaccinology and Molecular Diagnostics, School of Life Sciences, Xiamen University

Qingbing Zheng
Xiamen University https://orcid.org/0000-0002-7516-9965

Shuo Song
Southern University of Science and Technology

Chuanlai Yang
National Institute of Diagnostics and Vaccine Development in Infectious Diseases, School of Public Health, Xiamen University

Hua-Long Xiong
National Institute of Diagnostics and Vaccine Development in Infectious Diseases, School of Public Health & School of Life Science, Xiamen University

Sibo Zhang
State Key Laboratory of Molecular Vaccinology and Molecular Diagnostics, School of Life Sciences, Xiamen University

Minqing Hong
Xiamen University

Ya-Li Zhang
Xiamen University

Hai Yu
State Key Laboratory of Molecular Vaccinology and Molecular Diagnostics, School of Life Sciences, Xiamen University, Xiamen

Yuyun Zhang
Xiamen University

Hui Sun
Xiamen University

Yang Huang
Xiamen University

Tingting Deng

State Key Laboratory of Molecular Vaccinology and Molecular Diagnostics, School of Life Sciences, Xiamen University

Xin Chi

State Key Laboratory of Molecular Vaccinology and Molecular Diagnostics, School of Life Sciences, School of Public Health, Xiamen University, Xiamen, 361102

Jinjin Li

National Institute of Diagnostics and Vaccine Development in Infectious Disease, School of Public Health, Xiamen University, Xiamen

Shaojuan Wang

State Key Laboratory of Molecular Vaccinology and Molecular Diagnostics, School of Life Sciences, Xiamen University

Lizhi Zhou

Xiamen University

Tingting Chen

State Key Laboratory of Molecular Vaccinology and Molecular Diagnostics, School of Life Sciences, Xiamen University

Yingbin Wang

State Key Laboratory of Molecular Vaccinology and Molecular Diagnostics, School of Life Sciences, School of Public Health, Xiamen University, Xiamen, 361102

Tong Cheng

Xiamen University https://orcid.org/0000-0002-1638-6214

Tian-Ying Zhang

Xiamen University https://orcid.org/0000-0002-2477-329X

Quan Yuan

Xiamen University https://orcid.org/0000-0001-5487-561X

Qinjian Zhao

National Institute of Diagnostics and Vaccine Development in Infectious Disease, School of Public Health, Xiamen University, Xiamen, China 361102

Jun Zhang

Xiamen University

Jason McLellan

The University of Texas at Austin https://orcid.org/0000-0003-3991-542X

Z. Hong Zhou

University of California, Los Angeles https://orcid.org/0000-0002-8373-4717

Zheng Zhang

Institute for Hepatology, National Clinical Research Center for Infectious Disease, Shenzhen Third People's hospital https://orcid.org/0000-0002-3544-1389

Ying Gu

State Key Laboratory of Molecular Vaccinology and Molecular Diagnostics, School of Life Sciences, Xiamen University, Xiamen https://orcid.org/0000-0002-2870-2800

Shaowei Li (shaowei@xmu.edu.cn)

Xiamen University https://orcid.org/0000-0002-3374-1038

Ningshao Xia

Xiamen University https://orcid.org/0000-0003-0179-5266

Article

Keywords: SARS-CoV-2, COVID-19, variants, antibodies

Posted Date: June 11th, 2021

DOI: https://doi.org/10.21203/rs.3.rs-582977/v1

Version of Record: A version of this preprint was published at Nature Communications on September 27th, 2021. See the published version at https://doi.org/10.1038/s41467-021-25997-3.

Abstract

The emergence of numerous variants of SARS-CoV-2, the causative agent of COVID-19, has presented new challenges to the global efforts to control the still ravaging COVID-19 pandemic. Here, we obtain two cross-neutralizing antibodies (7D6 and 6D6) that target *Sarbecoviruses'* receptor binding domain (RBD) with sub-picomolar affinities and potently neutralize authentic SARS-CoV-2. Crystal structures show that both antibodies bind a cryptic site different from that recognized by existing antibodies and highly conserved across *Sarbecovirus* isolates. Binding of these two antibodies to the RBD clashes with the adjacent N-terminal domain and disrupts the viral spike. Significantly, both antibodies confer good mutation resistance to the currently circulating SARS-CoV-2 variants. Thus, our results have direct relevance to public health as options for passive antibody therapeutics and even active prophylactics, and can also inform the design of pan-sarbecovirus vaccines.

Main Text

Severe acute respiratory syndrome coronavirus 2 (SARS-CoV-2), responsible for the ongoing global coronavirus disease 2019 (COVID-19) pandemic, is the third human coronavirus to cause widespread infection [1], having already claimed nearly 3.5 million lives and contributed to over 168 million confirmed cases in 219 countries and territories as of 29 March 2021. This pandemic has drastically disrupted our normal life and devastated public health and global economy [1-3]. Convalescent antibodies have shown efficacies to treat COVID-19 caused by the original virus strain of SARS-CoV-2 [4,5]; as the only scientifically proven therapeutic measure to save lives, antibody cocktails have been clinically prescribed under Emergency Use Authorization (EUA) to patients, as in a well-publicized case [6]. More recently, several vaccines that confer excellent COVID-19 protection efficacy have been approved for vaccination for the purpose of herd immunity [7]. However, the emerging SARS-CoV-2 variants—largely attributed to the current (and more anticipated in the future) case resurgences in the US, Europe, South Africa and Brazil—evade immunity and reduced the efficacies of existing antibody cocktail treatment [8-10]. These variants potentially diminish the effectiveness of the approved vaccines and are poised to dash our hope for a quick returning to normalcy. For example, the Moderna (mRNA-1273), Pfizer (BNT162b2), and Novavax (NVX-CoV2373) vaccines show lower protection efficacy for these epidemic variants than the original strains [2,11]. A broadly protective vaccine that could prevent infection of known and future variants is thus urgently needed. Alternatively, broadly neutralizing antibodies could be used as both therapeutics and prophylactics [12,13]. Such antibodies can also be used to pinpoint highly conserved antigenic determinants across various coronavirus strains to guide design of a broad-spectrum vaccine. They can also serve as indicators for cross-protection potential upon vaccine immunization.

Efficient human-to-human coronavirus transmission is driven by the spike glycoprotein (S), which is located on the viral surface [14,15]. Each S monomer is proteolytically cleaved into S1 and S2 subunits prior to mediating virus entry into host cells by interacting with surface receptors [14,15]. Both SARS-CoV-2 and SARS-CoV enter host cells by engaging with the angiotensin-converting enzyme 2 (ACE2) receptor, which

is recognized by the receptor-binding domain (RBD) of S [15]. As S transitions from a prefusion to postfusion state, the RBD undergoes complex conformational changes from a closed to an open conformation [14,16,17]. Therefore, S protein and host factors related to cell entry of SARS-CoV-2 are promising targets for therapeutics development against COVID-19 [18-20]. Among reported potent neutralizing antibodies (nAbs), most neutralize coronaviruses by targeting the receptor binding motif (RBM) within the RBD to block S from engaging with ACE2 [5,21,22]. However, many of these nAbs are specific to either SARS-CoV-2 or SARS-CoV, and are unable to neutralize variant strains [8]. To date, at least two classes of cross-neutralizing antibodies have been identified: representative CR3022 [23,24] and S309 [25]. These nAbs recognize two non-overlapping conserved epitopes distal from the RBM. However, S309's neutralization activity was found to be impaired toward the UK variant [8], though whether CR3022's efficacy also suffers remains to be determined.

In this study, two cross-neutralizing antibodies, 7D6 and 6D6, were raised following immunization with the SARS-CoV-2 S-trimer alone (7D6) or in combination with the SARS-CoV S-trimer and MERS-CoV RBD (6D6). High-resolution crystal structures reveal that both antibodies target a distinctive cryptic site of the RBD with high conservation. Our results thus help expand the epitope coverage for antibody cocktail therapies to cope with emerging variants, and benefit our global efforts in designing pan-sarbecovirus vaccines.

Result

Cross-neutralizing antibodies elicited by combined immunization of coronavirus spikes

To obtain cross-neutralizing antibodies, we explored immune response through combined immunization of *Sarbecoviruses*. Mice were immunized with SARS-CoV-2 spike protein alone and in combination with the SARS-CoV spike protein and the MERS-CoV RBD [16] (Fig. 1A and 1B). The hybridoma cell pools with reactivities against both SARS-CoV-2 and SARS-CoV spikes were selected and screened for cross-reactive monoclonal antibodies (mAbs). We obtained 5 and 10 lead mAbs from the single and combined immunization strategies, respectively (Fig. 1C). Four of the five mAbs derived from the SARS-CoV-2 spike protein immunization recognized the S2 protein, whereas the fifth mAb targeted the RBD. Comparatively, for the combined immunization, only one recognized the S2 protein, whereas the remaining nine mAbs recognized the S1, eight of which targeted the RBD. These activity profiles suggest that the RBD is relatively more immunogenic than the S2 protein in terms of cross-reactive immunity (Fig. 1C and Table S1).

We next evaluated the neutralization potency of these 15 mAbs using the lentiviral virus (LV) [26] and vesicular stomatitis virus (VSV) pseudotyping systems [27]. A total 7 mAbs—one from the SARS-CoV-2 spike protein immunization and six from the *Sarbecovirus* spike immunization—showed cross-neutralizing activities against SARS-CoV-2 and SARS-CoV. Intriguingly, all seven cross-neutralizing mAbs recognized the RBD (Table S1). In terms of the holistic profiles of cross-reactivity and cross-neutralization,

three mAbs—7D6, 6D6 and 16D8— stood out as lead antibodies and conferred potent cross-neutralization as IC_{50} value ranging from 2.56 to 8.91 μg/ml for SARS-CoV-2 pseudotyped LV (LV-SARS-CoV-2), 1.21-10.11 μg /mL for LV-SARS-CoV and 0.04-0.26 μg/mL for VSV-SARS-CoV-2 (Fig. 2A to 2C). By contrast, the cross-neutralizing antibody CR3022 showed poor neutralizing activity against LV-SARS-CoV-2 (IC_{50} > 284 μg/mL) in our test (Fig. 2A).

Characterization of cross-neutralizing antibodies

We selected the three promising mAbs for further investigation—7D6 (raised by single immunization strategy), and 6D6 and 16D8 (raised by combined strategy)—and evaluated their neutralization activities using the SARS-CoV-2 authentic virus neutralization assay [5]. All three cross-neutralizing mAbs could potently neutralized SARS-CoV-2 with comparable IC_{50} values: 2.23, 1.77, and 5.30 μg/mL, respectively (Fig. 2D). Using surface plasmon resonance (SPR) analysis, we found that these neutralizing mAbs interacted with the two-proline stabilized S trimer (S-2P) and RBD with nanomolar or even picomolar affinities, for both SARS-CoV and SARS-CoV-2 strains (Fig. 2E and Table S2). Particularly, 7D6 bound to the RBD with a 2-log higher affinity than the trimeric S-2P, whereas 6D6, which showed comparable binding affinities to the two proteins, had 2-log higher affinities for SARS-CoV-2 proteins than SARS-CoV proteins (Fig. 2E). 16D8 showed similar affinity discrepancy as that of 7D6, and a similarly lower affinity to SARS-CoV as 6D6. A blocking assay further confirmed that 7D6 and 6D6 did not inhibit the binding between ACE2 and the RBD; 16D8, however, did block this interaction (Fig. 2F). Examining all three mAbs in an inter-blocking assay, we found that 6D6 could completely block 7D6 from binding to the RBD (Fig. 2G); 16D8 could block neither 7D6 nor 6D6 from engaging with the RBD. Collectively, these results suggest an overlap in the binding epitopes of 7D6 and 6D6 that are distinct from the RBM and binding site of most other mAbs as well as the 16D8 epitope, and that 16D8 may recognize a site associated with ACE2 binding.

Structural basis of 7D6/6D6 cross-neutralization

Next, we determined chemical bonds between these antibodies and SARS-CoV-2 spikes by solving the crystal structures of Fab-RBD immune-complexes. We obtained crystals of SARS-CoV-2 RBD bound with Fabs of either 7D6, 6D6 or 16D8 and solved the structures at 1.40 Å and 1.92 Å resolutions for RBD:7D6 and RBD:6D6 complexes, respectively (Fig. S1 and Table S3). We showed that 7D6 and 6D6 bind to a nearly identical region of the RBD in a similar orientation (Fig. 3A and 3D). This region is located at a site distal to the RBM (Fig. 3G), consistent with the results of the above SPR assay (Fig. 2F). The paratopes of 7D6 and 6D6 comprise 6 and 5 complementarity determining region (CDR) loops, respectively, with a buried area at the antibody-RBD interface of about 795.8 $Å^2$ (HCDRs accounting for 73.3%; LCDRs, 26.7%) and 1,019.1 $Å^2$ (HCDRs, 54.7%; LCDRs, 45.3%), respectively (Fig. 3B and 3E). The epitopes for 7D6 and 6D6 are formed by 21 and 25 residues, respectively, most of which located at η1, β1, β5 and β7-β8 loop of RBD, with 18 shared residues (Fig. 3C and 3F, Fig. S2). Furthermore, their binding sites on the spike of SARS-CoV-2 and SARS-CoV are highly conserved, with 16 (16/21, 76.2%) conserved residues for binding with 7D6, and 20 (20/25, 80%) conserved residues for 6D6 (Fig. S2). The 18 shared residues within the

epitope are highly conserved (91.5%) across *Sarbecovirus* isolates (Fig. 3H and Table S4); we denote this shared region as the 7D6/6D6 site.

7D6 interacts with the SARS-CoV-2 RBD mainly through eight hydrogen bonds and van der Waals force between HCDR1-3 and residues 346-355 and 466-471 of the RBD (Fig. 3I); RBD residues T470, Y351, R346, R466, Y102, and R355 are critical to their interactions (Fig. 3J). For 6D6, the binding site comprises predominantly two RBD segments, one from residues 351 through 357 and the other from residues 457 through 471 (Fig. 3K). A strong and extensive interaction network, including 15 hydrogen bonds and several van der Waals contacts, is formed between 6D6 and the RBD, with T470, Y351, R466, F464, R355, P463, R457, N460, E465, and R357 acting as key residues in the antigenic determinant (Fig. 3L). Among the critical residues in the 7D6 and 6D6 epitopes, there are five amino acid variations between SARS-CoV-2 and SARS-CoV (T470 in SARS-CoV-2 to N in SARS-CoV, R346àK, E471àV, N460àK, R357àK), but these variations do not substantially affect cross reactivity (Fig. 2A and 2B).

Mutation resistance of 7D6/6D6 and classification of SARS-CoV-2 RBD nAbs

Over the past year, antibody resistance has developed in SARS-CoV-2 variants, including B.1.1.7 (UK) and B.1.351 (South Africa) [8]. The major mutations have been identified to be predominantly within the RBM: N501Y in the UK variant; K417N/ E484K/N501Y in the South Africa variant [28]; K417T/E484K/N501Y in the Brazil variant and L452R in the California variant [29]. And all these mutation positions are located outside the 7D6/6D6 site (Fig. 4A). Expectedly, 7D6 and 6D6 maintain excellent reactivities against the RBD in proteins bearing these typical mutations as compared with the original strain (Fig. 4B), in contrast, COVID-19 convalescent sera exhibited lower reactivities to RBD mutants to various extents. Meanwhile, 7D6 and 6D6 show nearly unchanged neutralizing potency against LV-SARS-CoV-2 of the circulating B.1.1.7, B.1.351, P.1 variants, and as well as against the B.1.351 authentic virus. However, control REGN10933 exhibits significantly lower activity against LV-SARS-CoV-2 of B.1.351 and P.1, despite unchanged against B.1.1.7 (Fig. 4B and Fig. S3 to S4).

Based on binding orientation and footprint of 7D6/6D6 and other reported nAbs, RBD-targeting nAbs can be grouped into six classes (Class 1-6) (Fig. 4C). Antibodies in Class 1-3 are SARS-CoV-2 specific. Class 1, as represented by antibody CB6[5], which targets a region with a large overlapping area to the RBM, comprises a total of 21 reported Abs [4,5,21,22,30-39]. Class 2, represented by P2B-2F6 [5], which targets a reciprocal region that partially overlaps with the RBM, includes a total of 19 Abs [4,30,37,38,40-47]. Class 3 has three antibodies [36]; the footprint of the representative REGN10987 [4,32,36] is almost separate from the RBM. The binding epitopes for antibodies in Classes 1-3 overlap with the ACE2 binding site to various extents, and thus likely neutralize the virus by blocking ACE2 from binding to the RBD. Antibodies in Class 4 and 5 bind two separate regions distal to the RBM. Class 4 has a total of 8 antibodies including 4 cross-neutralizing ones [23,38,45,48-51]; the well-known CR3022 targets a cryptic epitope on the outer side of the RBD and may cause neutralization by antibody-induced spike disruption [24]. Class 5 includes to-date one antibody, S309 [25], which has a footprint distinct from the RBM and the CR3022 epitope. S309 neutralizes

the virus via multiple mechanisms, such as antibody-dependent cell cytotoxicity (ADCC) and antibody-dependent cellular phagocytosis (ADCP). As the 7D6/6D6 site presented in this study is in a distinct and cryptic position, away from the binding regions of the other classes and the RBM, we propose 7D6 and 6D6 as a new class, Class 6, and may exert its neutralization by destabilization of the trimeric spike (Fig. 4C and 4D, Table S5). For COVID-19 therapy, the passive treatment of individual antibodies or non-competing antibody cocktails is an effective approach, and three kinds of antibodies or combos have been approved under Emergency Use Authorization (EUA) (Fig 4E), although these show lower efficacies to the emerging variants to some extent [8-10]. 7D6 and 6D6 bind a highly conserved site different from all these clinical antibodies (Fig. 4E), thus their appropriate humanized forms could be a potential candidate or an enhancer to existing cocktails to combat variants.

Mechanism of 7D6/6D6-mediated neutralization

We next individually fitted the two immune-complex structures to the RBD in both its open and closed conformation in the structure of the trimeric spike, and found that, in all interaction scenarios, the bound Fabs would clash with the adjacent NTDs (Fig. 5A, 5B, 5E, 5F, 5I, 5J, 5M and 5N). The overlapping volumes of 7D6 to the adjacent NTD in the fitted models were 3,700 A^3 for RBD up and 11,800A^3 for RBD down, and the occlusion volumes for 6D6 were 3,700 A^3 (RBD up) and 13,100 A^3 (RBD down) (Fig. 5C, 5G, 5K and 5O). Therefore, the 7D6/6D6 site, located on the inner aspect of the RBD facing the adjacent NTD, is cryptic in the context of the entire trimeric spike (Fig. 5D, 5H, 5L and 5P).

Following this, we investigated binding of 7D6 or 6D6 to S-2P *in vitro*. High-performance liquid chromatography (HPLC) analysis showed that S-2P incubated with 7D6 or 6D6 Fab is split into smaller components while binding with the Fab (Fig. 6A, Fig. S5). Cryo-electron microscopy imaging of S-2P in complex with 7D6 or 6D6 Fab and 2D classification analyses of the resulting complexes confirmed antibody-mediated disruption of the trimeric spike (Fig. 6B and 6C).

Discussion

Regarding to viral neutralization mechanism, the established SARS-CoV-2 cross-neutralizing antibody CR3022 provides neutralization through antibody-induced spike disruption [24]. Similarly, we previously showed that the 8C11 antibody can neutralize native Hepatitis E virus (HEV) by antibody-imposed physical disruption [52]. Indeed, although the 7D6/6D6 site is inaccessible for antibody binding to the trimeric spike, 7D6 and 6D6 could still associate with the S-2P protein with excellent affinities (Fig. 2E), which suggests that the RBD might spatially relate to the NTD in a dynamic manner, thereby allowing the antibody to bind upon transient exposure of the 7D6/6D6 site. In other words, this cryptic 7D6/6D6 site may be a ‘breathing’ epitope—a concealed epitope that is exposed transiently with inter-domain movement—that has been also found in the hemagglutinin of the influenza virus [53,54]. To our knowledge, we propose 7D6/6D6 might neutralize virus by spike destabilization from ACE2 binding or S1 shedding mechanism (Fig. 6C).

Currently, numbers of COVID-19 vaccines are available and over 200 candidates are under development, mostly using the gene of original SARS-CoV-2 strain[7]. Unfortunately, SARS-CoV-2 rapidly evolves out various variants that significantly diminish the efficacy for both vaccines and antibody therapeutics[8,11]. Thus, improved countermeasures for current and even future variants are urgently needed. This study demonstrates that combined immunization of *Sarbecoviruses* spikes produced more cross-neutralizing antibodies than the single immunization of SARS-CoV-2 spike. Vaccination regiments through combined and/or sequential immunization strategy could provide cross-immunity upon SARS-CoV-2 and SARS-CoV-1 as well as circulating variants by virtue of the cross-neutralizing antibody response, for instance from the 7D6/6D6 site that is highly conserved across *Sarbecovirus* isolates. Furthermore, the combined immunization strategy suggests that cross-neutralizing antibody would be readily produced in the convalescent COVID-19 patients who have recovered from the superinfection of original SARS-CoV-2 and some variants. It is supposed that more potent cross-neutralizing antibodies rather than nAbs Class 4-6 will be screened out from those convalescent individuals and applied to improve the efficacy and mutation resistance of antibodies or cocktails against current and future variants.

To curb the pandemic, wide-spectrum vaccine is an appealing means to establish herd immunity and good tolerance against emerging variants. The information of various conserved sites and extensive antibody-mediated neutralization mechanisms are essentially contributory to the vaccine design for broad protection[52,53,55]. Here, the discovery of 7D6/6D6 site showcases the effort to benefit for the development of pan-coronavirus vaccines, for example, 7D6 and 6D6 recognize the conserved epitopes on RBD different from that of other existing antibodies, have distinctive neutralization mechanism by spike destabilization (like CR3022)[23] and none ACE2 blocking (like S309)[25], and show good resistance to the UK, BZ, and SA strains. On the other hand, 7D6 and 6D6 per se require further modifications—such as mouse-human chimeric grafting, humanized engineering and affinity maturation—to satisfy clinical practical utilities, and their protection efficacy *in vivo* need to be verified. Meanwhile, how to expose the cryptic 7D6/6D6 site in immunogen design and make the epitope more immune focusing deserves more efforts towards a successful pan-coronavirus development.

In summary, our study shows the potential of SARS-CoV-2 cross-neutralizing antibodies developed using a combined immunization strategy. Two lead cross-neutralizing antibodies, 7D6 and 6D6, exhibit excellent picomolar affinities upon binding to the RBD and cross-neutralize against SARS-CoV-2 and SARS-CoV by targeting a highly conserved cryptic site within the RBD. These two antibodies impart neutralization by clashing with the neighboring NTD and thereby physically disrupting the spike complex. The unchanged reactivities of 7D6/6D6 against RBDs of currently circulating SARS-CoV-2 variants suggest that 7D6/6D6 could be promising candidates for antibody treatment related to virus variation. Their antigenic region uncovered here could be an ideal target for rational design of pan-sarbecovirus vaccines.

Materials And Methods

Ethics statement

All procedures in this study involving the authentic COVID-19 virus were performed in a biosafety level 3 (BSL-3) facility of the Shenzhen Third People's Hospital, China. The experimental protocols were approved by the Xiamen University Laboratory Animal Management Ethics Committee. All manipulations were strictly conducted in compliance with animal ethics guidelines and approved protocols.

Cell lines

Cell lines used in this study were obtained from the ATCC (H1299, BHK21, Vero E6) or Thermo Fisher Scientific Inc. (CHO, 293T, sf9 and H5 cells). All cell lines used in this study were routinely tested for mycoplasma and found to be mycoplasma-free.

Cloning, protein expression and purification of S*arbecovirus* S-related proteins

The SARS-CoV-2, SARS-CoV, MERS-CoV S-2P proteins and/or RBDs were prepared as previously described[16]. In brief, the S genes (from the sequences of Genbank accession nos. NC_045512.2, NC_004718.3 and AFY13307.1 corresponding to SARS-CoV-2, SARS-CoV and MERS-CoV, respectively) were synthesized and individually cloned into a baculovirus shuttle vector pAcgp67B (BD Biosciences, CA, USA) using Gibson assembly. The expression and purification of S-2P and RBD constructs were performed as described previously[16]. Hive Five cells (BTI-TN-5B1-4) (Thermo Fisher Scientific) were cultured in ESF921 medium (Expression Systems) and infected with recombinant virus at a multiplicity of infection (MOI) of 5 in the exponential growth phase (2×10^6 cells/mL; 95% viability) at 28°C for 72 h. The culture media was centrifugated at 8,000 rpm for 20 min. The supernatant was dialyzed against phosphate-buffered saline (PBS), pH 7.4, purified with Ni-sepharose fast-flow 6 resin (GE Healthcare, Boston, USA), and eluted with 250 mM imidazole. The protein concentrations of the final purified samples were measured with Pierce BCA Protein Assay Kit (Thermo Fisher Scientific). The SARS-CoV-2 RBD mutants (N501Y, L452R, K417T/E484K/N501Y) were purchased from Sino Biological Inc. (Beijing, China).

Monoclonal antibodies (mAbs)

The immune scheme for mAb production was described by us elsewhere[16]. MAbs were prepared following standard hybridoma technology, as previously described[56]. Fusion was performed 2 weeks after the final immunization. The resulting hybridomas were screened for the secretion of SARS-CoV-2– and SARS-CoV–specific mAbs using a S-2P binding assay. Hybridoma cells were cloned using limiting dilution at least three times, and positive clones were expanded and cultured in 75-cm^2 flasks. MAbs were prepared by injecting hybridoma cells into the peritoneal cavities of pristine-primed BALB/c mice; ascites was collected after 9-12 days and stored at -20°C. MAbs were purified from mouse ascites using protein A agarose columns (GE Healthcare).

Expression and purification of IgG

The variable domain genes of CR3022[23] and REGN10933[36] heavy and light chains were inserted into a pTT5 (Thermo Fisher Scientific) vector containing the constant region of the human IgG. The

recombinant antibodies were expressed in Chinese hamster ovary (CHO) cells through transient transfection and purified from culture media by affinity chromatography using MabSelect Sure resin (GE Healthcare).

SDS-PAGE

Protein samples were mixed with loading buffer (50 mM Tris pH 6.8, 2% SDS, 5% 2-mercaptoethanol, 0.01% bromophenol blue, 8% glycerol), boiled for 10 min, and subjected to sodium dodecyl sulfate-polyacrylamide gel electrophoresis (SDS-PAGE). Equal amounts of protein for each sample were loaded onto SDS-PAGE gels. The proteins were electrophoresed for 70 min at 120 V in a BioRad MINI-PROTEAN Tetra system (BioRad Laboratories, CA, USA), and the gel was stained with Coomassie Brilliant Blue R-250 (Bio-Rad) for 30 min at room temperature.

Enzyme-Linked Immunosorbent Assay (ELISA)

Purified proteins were coated into the wells of 96-well microtiter plates at 100 ng/well in PBS and incubated at 37°C for 4 h. The background was blocked with 1 × enzyme dilution buffer (PBS + 0.25% casein + 1% gelatin + 0.05% proclin-300) at 37°C for 2 h. Antibodies or Sera at 2 μg/mL or 1:100 respectively was three-fold serially diluted, added to the wells (100 μL), and incubated at 37°C for 1 h. A horseradish peroxidase (HRP)-labeled goat anti-mouse or goat anti-human antibody (Abcam) was used as the secondary antibody at 1:5,000 for 30 min. Wells were washed again and the reaction catalyzed using o-phenylenediamine (OPD) substrate at 37°C for 10 min. The OD450 nm (reference, OD620 nm) was measured on a microplate reader (TECAN, Männedorf, Switzerland) with a cut-off value of 0.1. The half-effective concentration (EC_{50}) or half-effective titers (ET_{50}) was calculated by sigmoid trend fitting using GraphPad Prism software (GraphPad Software, CA, USG).

SARS-CoV-2 neutralization assay

SARS-CoV-2 live virus focus reduction neutralization test (FRNT) was performed in a certified Biosafety level 3 laboratory, as previously described[5]. Neutralization assays against live SARS-CoV-2 were conducted using a clinical isolate (EPI_ISL_406594 (WT), EPI_ISL_1205467 (B.1.351) at GISAID) previously obtained from a nasopharyngeal swab of an infected patient. Serial dilutions of tested antibodies were mixed with 50 μL of SARS-CoV-2 (100 focus forming units) in 96-well microwell plates and incubated at 37 °C for 1 h. Mixtures were then transferred to 96-well plates seeded with Vero E6 cells and allowed to absorb for 1 h at 37°C. Inoculums were removed before adding the overlay media (100 μL MEM containing 1.6% carboxymethylcellulose). The plates were then incubated at 37°C for 24 h. Overlays were removed and then cells were fixed with 4% paraformaldehyde solution for 30 min, and permeabilized with Perm/Wash buffer (BD Biosciences) containing 0.1% Triton X-100 for 10 min. Cells were incubated with rabbit anti-SARS-CoV-2 NP IgG (Sino Biological, Inc) for 1 h at room temperature followed by HRP-conjugated goat anti-rabbit IgG (H+L) antibody (TransGen Biotech, Beijing). The reactions were developed with KPL TrueBlue Peroxidase substrates (Seracare Life Sciences Inc). The numbers of SARS-CoV-2 foci were calculated using an EliSpot reader (Cellular Technology Ltd).

Pseudotype LV-based neutralization test

Antibodies were tested against lentiviral pseudotyping particles (LVpp) bearing the SARS-CoV-2 spike antigen based on H1299-ACE2hR cells, as described previously[26]. In briefly, SARS-CoV-2 LVpp were generated by co-transfection of a lentiviral packaging plasmid (psPAX2, Addgene), a SARS-CoV-2 spike expression plasmid (containing codon-optimized spike gene derived from the strain of MN908947.3 (WT) or EPI_ISI_601443 (B.1.1.7) or EPI_ISI_700428 (B.1.351) or EPI_ISI_792680 (P.1)) and a green fluorescent protein (mNeonGreen) reporter vector (pLvEF1α-mNG, carrying EF1α promoter-driven mNeonGreen expressing cassette) in 293T cells. Infection and neutralization assays were performed on H1299-ACE2hR cells, which stably over-expressed human ACE2 (enabling it is highly susceptible to SARS-CoV-2 virus) and nuclear-localized RFP (H2B-mRuby3, allowing accurate cell counting) based on H1299 cells. For ppNAT tests, serially-diluted antibodies were incubated with LVpp inoculum (0.5 TU/cell) for 1 hour. Subsequently, the mixtures were incubated with the cells, which had been pre-seeded in 96-well cell culture plates with an optically-clear bottom. After 36-hour incubation, the plates were imaged by using Opera Phenix or Operetta CLS high-content equipment (PerkinElmer). For quantitative determination, fluorescence images were analyzed by Columbus Software 2.5.0 (PerkinElmer), the numbers of mNeonGreen (+) cells per well were calculated to indicate the infection performance, and the total cell numbers per well were also counted to normalize the readouts. The reduction (%) on mNeonGreen (+) cells of the plasma-treated well in comparison with control-well was calculated to show the neutralization activity. The ppNAT titer of each samples were expressed as the maximum dilution concentration required to achieve infection inhibition by 50% (IC_{50}). The IC_{50} value was determined by the 4-parameter logistic (4PL) regression using GraphPad Prism v8.0.

Pseudotype VSV-based neutralization test

The VSV-based neutralization test was carried out as described[27]. The cultured supernatant of the monoclonal hybridoma cells and gradient-diluted purified antibodies were mixed with diluted VSVSARS-CoV-2-Sdel18 virus (MOI=0.05) and incubated at 37°C for 1 h. All samples and viruses were diluted with 10% FBS-DMEM. The mixture was added to pre-seeded BHK21-hACE2 cells. After incubating for 12 h, fluorescence images were obtained with Opera Phenix or Operetta CLS equipment (PerkinElmer). For quantitative analysis, fluorescence images were analyzed using the Columbus system (PerkinElmer), and the numbers of GFP-positive cells for each well were counted to represent infection performance. The reduction (%) in the number of GFP-positive cells in mAb-treated wells compared with that in nontreated control wells were calculated to show the neutralizing potency.

Size-Exclusive Chromatography (SEC)

All high-purity RBD, Fab and immune complex proteins were subjected to HPLC (Waters; Milford, MA) analysis using a TSK Gel G5000PWXL7.8 × 300- mm column (TOSOH, Tokyo, Japan) equilibrated in PBS, pH 7.4. The system flow rate was maintained at 0.5 mL/min and eluted proteins were detected at 280 nm.

K_D determination

K_D values were determined by SPR technology using a Biacore 8K instrument (GE Healthcare). The S-2P or RBD was amine-coupled to a CM-5 sensor chip for use. Antibodies was then captured on the sensor surface at a flow rate of 30 μL/min in PBS-P+ buffer (0.2 M phosphate buffer with 27 mM KCl, 1.37 M NaCl, and 0.5% Surfactant P20 (Tween 20)). The antibodies were tested using serially diluted concentrations (200, 150, 100, 75, 50, 37.5, 25, 18.75, 12.5, and 9.375 nM). The flow durations were 200 s for the association stage and 10 min for dissociation. Association rates (ka), dissociation rates (kd), and affinity constants (K_D) were calculated using BIAcore evaluation software.

Blocking assay

A blocking assay was carried out to investigate the binding mode of the monoclonal antibodies with hACE2 (or between two antibodies) using SPR technology in a Biacore 8K instrument (GE healthcare). All experiments were performed at 25°C, and the biosensors were pre-equilibrated in PBS-P+ buffer (0.2 M phosphate buffer with 27 mM KCl, 1.37 M NaCl and 0.5% Surfactant P20 [Tween 20]) for 10 min. Antibodies (first protein) at 3000 nM were loaded onto the biosensors for 500 s, followed by flow of the second interacting protein (hACE2 or the second antibody), also at 3000 nM for 500 s. The unblocked pattern of the RBD with buffer was used as a control.

Preparation, crystallization, and structure determination of immune complexes

7D6, 6D6 and 16D8 Fabs were prepared by papain digestion of the mAb and purified with Protein A (GE Healthcare). The SARS-CoV-2 RBD was mixed with each Fab in a 1:1.2 molar ratio and incubated at 37°C for 2 h. The immune complex was further purified to remove any excess Fab by gel filtration on a Superdex 200 Increase column (GE Healthcare) in 10 mM Tris pH 8.0 with 50 mM NaCl. The complex was concentrated to ~7.5 mg/mL for crystallization.

The crystallization was performed using sitting-drop vapor diffusion in the screening stage and hanging drop in microseeding optimization at 20°C. Crystals of the 7D6:RBD complex were grown in 0.2 M potassium dihydrogen phosphate with 20% PEG3350, whereas crystals of the 6D6:RBD complex were grown in 0.2 M sodium thiocyanate with 20% PEG3350. Crystal growth took about 7 days before final data collection. Crystals were cryo-protected in reservoir solution supplemented with 30% glycerol at 100 K before collection of the diffraction data. Diffraction data were collected at Shanghai Synchrotron Radiation Facility (SSRF) beamline BL17U1 using a DECTRIS EIGER X 16M Detector (wavelength, 0.97919Å). The diffraction data were auto-processed by aquarium pipeline[57]. The complex structures were determined by the molecular replacement method using Phaser[58]. The search model for RBD, 7D6 Fab and 6D6 Fab phasing are COVID-19 RBD structure (PDB no. 6M0J), Fab structure in PDB no. 6RCO and Fab structure in PDB no. 1WEJ, respectively. The resulting models were manually built in COOT[59], refined with PHENIX[60] and analysed with MolProbity[61]. In brief, one round of rigid-body refinement was performed after molecular replacement phasing. The refined models were manually modified in COOT;

coordinates and individual B factors were refined in reciprocal space. TLS refinement was performed in the later stages with auto-searched TLS groups in PHENIX, which were listed in REMARK 3 sections in the deposited cif files. Data collection and structure refinement statistics were summarised in **Table S3**. All figures were prepared with PyMoL Molecular Graphics System (https://pymol.org).

Sequence and conservation analysis of epitopes

SARS-CoV-2 S gene mutations were calculated based on those within GISAID (https://www.gisaid.org) on 8 March 2021 (n = 415,516). SARS-CoV S genes were sourced from ViPR (https://www.viprbrc.org) using only those deposited before December 2019 to exclude SARS-CoV-2 (search criteria: SARS-related coronavirus, full-length genomes, all host; n = 85, performed on 15 March 2021). Pangolin sequences were sourced from GISAID (n = 9). Reported for percent conservation are the number of sequences with an identical change at a position divided by the total number of sequences. The conservation figure indicating the sequence conservation was generated using PyMoL Molecular Graphics System.

Preparation and data collection of Cryo-EM samples

Aliquots (3 μL) of 0.5 mg/mL purified S-2P protein or its immune-complexes were loaded onto glow-discharged (60 s at 20 mA) holey carbon Quantifoil grids (R1.2/1.3, 200 mesh, Quantifoil Micro Tools) using a Vitrobot Mark IV (Thermo Fisher Scientific) at 100% humidity and 4°C. Data were acquired using the EPU software on an FEI Tecnai F30 transmission electron microscope (Thermo Fisher Scientific) operated at 300 kV and equipped with a Thermo Fisher Falcon-3 direct detector. Images were recorded in the 39-frame movie mode at a nominal magnification of 93,000× with a pixel size of 1.12 Å on the sample level and an underfocus range of 1.5 to 2.8 μm. The total electron dose was set to 30 e^{-} $Å^{-2}$ and the exposure time was 1.0 s.

Cryo-EM data processing

Movie frame alignment and contrast transfer function estimation of each aligned micrograph were carried out with the programs of Motioncor[62] and Gctf[63]. Particles were picked by the “Template picker” session of CryoSPARC v2[64]. Two rounds of reference-free 2D classification were performed, and well-defined particle images were selected.

Declarations

Acknowledgments: We thank Dr. Huan Zhou (beamline BL17U1 at the Shanghai Synchrotron Radiation Facility) for the assistance in X-ray data collection and processing.

Funding:

This work was supported by grants from the National Natural Science Foundation (grant nos. 81991491, 82001756, U1705283), the National Key Research and Development Program of China (grant no. 2020YFC0842600), the Science and Technology Major Projects of Xiamen (grant no. 3502Z20203023).

Author contributions:

Z.H.Z., Z.Z., Y.G., S.L. and N.X. designed the study. T.L., W.X., Q.Zheng, S.S., C.Y., H.X., S.Z., M.H., Yali.Z, Yuyun Z., , H.S., Y.H., T.D. X.C., J.L., S.W., L.Z., and T.Chen performed experiments. T.L., W.H., Q.Zheng, H.Y., Y.G., S.L. and N.X. analyzed data. T.L., Q.Z., J.S.M., Z.H.Z., Y.G., and S.L. wrote the manuscript. T.L., W.X., Q.Zheng, Y.W., T.Cheng, T.Z., Q.Y., Q.Zhao, Z.H.Z., J.Z., Y.G., S.L., and N.X. participated in discussion and interpretation of the results. All authors contributed to experimental design.

Competing interests: No potential conflict of interest was reported by the author(s).

Data and materials availability:

The coordinates and structure factors for 7D6:RBD, 6D6:RBD have been deposited in the Protein Data Bank (accession nos. 7EAM, 7EAN).

References

1 Zhou, P. *et al.* A pneumonia outbreak associated with a new coronavirus of probable bat origin. *Nature* **579**, 270-273, (2020).

2 Burki, T. Understanding variants of SARS-CoV-2. *Lancet* **397**, 462, (2021).

3 Wang, C., Horby, P. W., Hayden, F. G. & Gao, G. F. A novel coronavirus outbreak of global health concern. *Lancet* **395**, 470-473, (2020).

4 Barnes, C. O. *et al.* SARS-CoV-2 neutralizing antibody structures inform therapeutic strategies. *Nature* **588**, 682-687, (2020).

5 Ju, B. *et al.* Human neutralizing antibodies elicited by SARS-CoV-2 infection. *Nature* **584**, 115-119, (2020).

6 Thomas, K. & Kolata, G. *President Trump Received Experimental Antibody treatment*, <https://www.nytimes.com/2020/10/02/health/trump-antibody-treatment.html> (2020).

7 Li, T., Zhang, T., Gu, Y., Li, S. & Xia, N. Current Progress and Challenges in the Design and Development of a Successful COVID-19 Vaccine. *Fundamental Research* **1**, 139-150, (2021).

8 Wang, P. *et al.* Antibody Resistance of SARS-CoV-2 Variants B.1.351 and B.1.1.7. *Nature*, 1-9, (2021).

9 Hoffmann, M. *et al.* SARS-CoV-2 variants B.1.351 and P.1 escape from neutralizing antibodies. *Cell*, (2021).

10 Wang, P. *et al.* Increased Resistance of SARS-CoV-2 Variant P.1 to Antibody Neutralization. *bioRxiv*, 2021.2003.2001.433466, (2021).

11 Garcia-Beltran, W. F. *et al.* Multiple SARS-CoV-2 variants escape neutralization by vaccine-induced humoral immunity. *Cell*, (2021).

12 Saphire, E. O. *et al.* Crystal Structure of a Neutralizing Human IgG Against HIV-1: A Template for Vaccine Design. *Science* **293**, 1155-1159, (2001).

13 Laursen, N. S. *et al.* Universal protection against influenza infection by a multidomain antibody to influenza hemagglutinin. *Science* **362**, 598-602, (2018).

14 Hoffmann, M. *et al.* SARS-CoV-2 Cell Entry Depends on ACE2 and TMPRSS2 and Is Blocked by a Clinically Proven Protease Inhibitor. *Cell* **181**, 271-280.e278, (2020).

15 Matheson, N. J. & Lehner, P. J. How does SARS-CoV-2 cause COVID-19? *Science* **369**, 510-511, (2020).

16 Wrapp, D. *et al.* Cryo-EM structure of the 2019-nCoV spike in the prefusion conformation. *Science* **367**, 1260-1263, (2020).

17 Shang, J. *et al.* Cell entry mechanisms of SARS-CoV-2. *Proc National Acad Sci* **117**, 11727-11734, (2020).

18 Walls, A. C. *et al.* Unexpected Receptor Functional Mimicry Elucidates Activation of Coronavirus Fusion. *Cell* **176**, 1026-1039.e1015, (2019).

19 Bruchez, A. *et al.* MHC class II transactivator CIITA induces cell resistance to Ebola virus and SARS-like coronaviruses. *Science* **370**, 241, (2020).

20 Wells, A. I. & Coyne, C. B. Inhibiting Ebola virus and SARS-CoV-2 entry. *Science* **370**, 167, (2020).

21 Wu, Y. *et al.* A noncompeting pair of human neutralizing antibodies block COVID-19 virus binding to its receptor ACE2. *Science* **368**, 1274-1278, (2020).

22 Yuan, M. *et al.* Structural basis of a shared antibody response to SARS-CoV-2. *Science* **369**, 1119-1123, (2020).

23 Yuan, M. *et al.* A highly conserved cryptic epitope in the receptor binding domains of SARS-CoV-2 and SARS-CoV. *Science* **368**, 630-633, (2020).

24 Huo, J. *et al.* Neutralization of SARS-CoV-2 by Destruction of the Prefusion Spike. *Cell Host Microbe* **28**, 445-454.e446, (2020).

25 Pinto, D. *et al.* Cross-neutralization of SARS-CoV-2 by a human monoclonal SARS-CoV antibody. *Nature* **583**, 290-295, (2020).

26 Chang, L. *et al.* The prevalence of antibodies to SARS-CoV-2 among blood donors in China. *Nat Commun* **12**, 1383, (2021).

27 Xiong, H.-L. *et al.* Robust neutralization assay based on SARS-CoV-2 S-protein-bearing vesicular stomatitis virus (VSV) pseudovirus and ACE2-overexpressing BHK21 cells. *Emerg Microbes Infec* **9**, 2105-2113, (2020).

28 Tegally, H. *et al.* Emergence of a SARS-CoV-2 variant of concern with mutations in spike glycoprotein. *Nature*, 1-8, (2021).

29 Li, Q. *et al.* The Impact of Mutations in SARS-CoV-2 Spike on Viral Infectivity and Antigenicity. *Cell* **182**, 1284-1294.e1289, (2020).

30 Du, S. *et al.* Structurally Resolved SARS-CoV-2 Antibody Shows High Efficacy in Severely Infected Hamsters and Provides a Potent Cocktail Pairing Strategy. *Cell* **183**, 1013-1023.e1013, (2020).

31 Clark, S. A. *et al.* Molecular basis for a germline-biased neutralizing antibody response to SARS-CoV-2. *bioRxiv*, 2020.2011.2013.381533, (2020).

32 Tortorici, M. A. *et al.* Ultrapotent human antibodies protect against SARS-CoV-2 challenge via multiple mechanisms. *Science* **370**, 950-957, (2020).

33 Schoof, M. *et al.* An ultrapotent synthetic nanobody neutralizes SARS-CoV-2 by stabilizing inactive Spike. *Science* **370**, 1473-1479, (2020).

34 Barnes, C. O. *et al.* Structures of Human Antibodies Bound to SARS-CoV-2 Spike Reveal Common Epitopes and Recurrent Features of Antibodies. *Cell* **182**, 828-842.e816, (2020).

35 Hurlburt, N. K. *et al.* Structural basis for potent neutralization of SARS-CoV-2 and role of antibody affinity maturation. *bioRxiv*, 2020.2006.2012.148692, (2020).

36 Hansen, J. *et al.* Studies in humanized mice and convalescent humans yield a SARS-CoV-2 antibody cocktail. *Science* **369**, 1010-1014, (2020).

37 Kreye, J. *et al.* A Therapeutic Non-self-reactive SARS-CoV-2 Antibody Protects from Lung Pathology in a COVID-19 Hamster Model. *Cell* **183**, 1058-1069.e1019, (2020).

38 Piccoli, L. *et al.* Mapping Neutralizing and Immunodominant Sites on the SARS-CoV-2 Spike Receptor-Binding Domain by Structure-Guided High-Resolution Serology. *Cell* **183**, 1024-1042.e1021, (2020).

39 Bertoglio, F. *et al.* A SARS-CoV-2 neutralizing antibody selected from COVID-19 patients by phage display is binding to the ACE2-RBD interface and is tolerant to known RBD mutations. *bioRxiv*, 409318, (2020).

40 Liu, L. *et al.* Potent neutralizing antibodies against multiple epitopes on SARS-CoV-2 spike. *Nature* **584**, 450-456, (2020).

41 Hanke, L. *et al.* An alpaca nanobody neutralizes SARS-CoV-2 by blocking receptor interaction. *Nat Commun* **11**, 4420, (2020).

42 Custódio, T. F. *et al.* Selection, biophysical and structural analysis of synthetic nanobodies that effectively neutralize SARS-CoV-2. *Nat Commun* **11**, 5588, (2020).

43 Xiang, Y. *et al.* Versatile and multivalent nanobodies efficiently neutralize SARS-CoV-2. *Science* **370**, 1479-1484, (2020).

44 Wang, N. *et al.* Structure-based development of human antibody cocktails against SARS-CoV-2. *Cell Res* **31**, 101-103, (2021).

45 Zhang, C. *et al.* Development and structural basis of a two-MAb cocktail for treating SARS-CoV-2 infections. *Nat Commun* **12**, 264, (2021).

46 Huo, J. *et al.* Neutralizing nanobodies bind SARS-CoV-2 spike RBD and block interaction with ACE2. *Nat Struct Mol Biol* **27**, 846-854, (2020).

47 Jones, B. E. *et al.* LY-CoV555, a rapidly isolated potent neutralizing antibody, provides protection in a non-human primate model of SARS-CoV-2 infection. *bioRxiv*, 2020.2009.2030.318972, (2020).

48 Zhou, D. *et al.* Structural basis for the neutralization of SARS-CoV-2 by an antibody from a convalescent patient. *Nat Struct Mol Biol* **27**, 950-958, (2020).

49 Wrapp, D. *et al.* Structural Basis for Potent Neutralization of Betacoronaviruses by Single-Domain Camelid Antibodies. *Cell* **181**, 1436-1441, (2020).

50 Lv, Z. *et al.* Structural basis for neutralization of SARS-CoV-2 and SARS-CoV by a potent therapeutic antibody. *Science* **369**, 1505-1509, (2020).

51 Liu, H. *et al.* Cross-Neutralization of a SARS-CoV-2 Antibody to a Functionally Conserved Site Is Mediated by Avidity. *Immunity* **53**, 1272-1280.e1275, (2020).

52 Zheng, Q. *et al.* Viral neutralization by antibody-imposed physical disruption. *Proceedings of the National Academy of Sciences of the United States of America* **116**, 26933-26940, (2019).

53 Bangaru, S. *et al.* A Site of Vulnerability on the Influenza Virus Hemagglutinin Head Domain Trimer Interface. *Cell* **177**, 1136-1152.e1118, (2019).

54 Watanabe, A. *et al.* Antibodies to a Conserved Influenza Head Interface Epitope Protect by an IgG Subtype-Dependent Mechanism. *Cell* **177**, 1124-1135.e1116, (2019).

55 Shen, C. *et al.* A multimechanistic antibody targeting the receptor binding site potently cross-protects against influenza B viruses. *Science Translational Medicine* **9**, eaam5752, (2017).

56 Vare?ková, E. *et al.* Preparation of monoclonal antibodies for the diagnosis of influenza A infection using different immunization protocols. **180**, 107-116, (1995).

57 Yu, F. *et al.* Aquarium: an automatic data-processing and experiment information management system for biological macromolecular crystallography beamlines. *Journal of Applied Crystallography* **52**, 472-477, (2019).

58 McCoy, A. J. *et al.* Phaser crystallographic software. *Journal of Applied Crystallography* **40**, 658-674, (2007).

59 Emsley, P. & Cowtan, K. Coot: model-building tools for molecular graphics. *Acta crystallographica. Section D, Biological crystallography* **60**, 2126-2132, (2004).

60 Adams, P. D. *et al.* PHENIX: a comprehensive Python-based system for macromolecular structure solution. *Acta crystallographica. Section D, Biological crystallography* **66**, 213-221, (2010).

61 Chen, V. B. *et al.* MolProbity: all-atom structure validation for macromolecular crystallography. *Acta crystallographica. Section D, Biological crystallography* **66**, 12-21, (2010).

62 Zheng, S. Q. *et al.* MotionCor2: anisotropic correction of beam-induced motion for improved cryo-electron microscopy. *Nature methods* **14**, 331, (2017).

63 Zhang, K. Gctf: Real-time CTF determination and correction. *Journal of structural biology* **193**, 1-12, (2016).

64 Punjani, A., Rubinstein, J. L., Fleet, D. J. & Brubaker, M. A. cryoSPARC: algorithms for rapid unsupervised cryo-EM structure determination. *Nat Methods* **14**, 290-296, (2017).

Figures

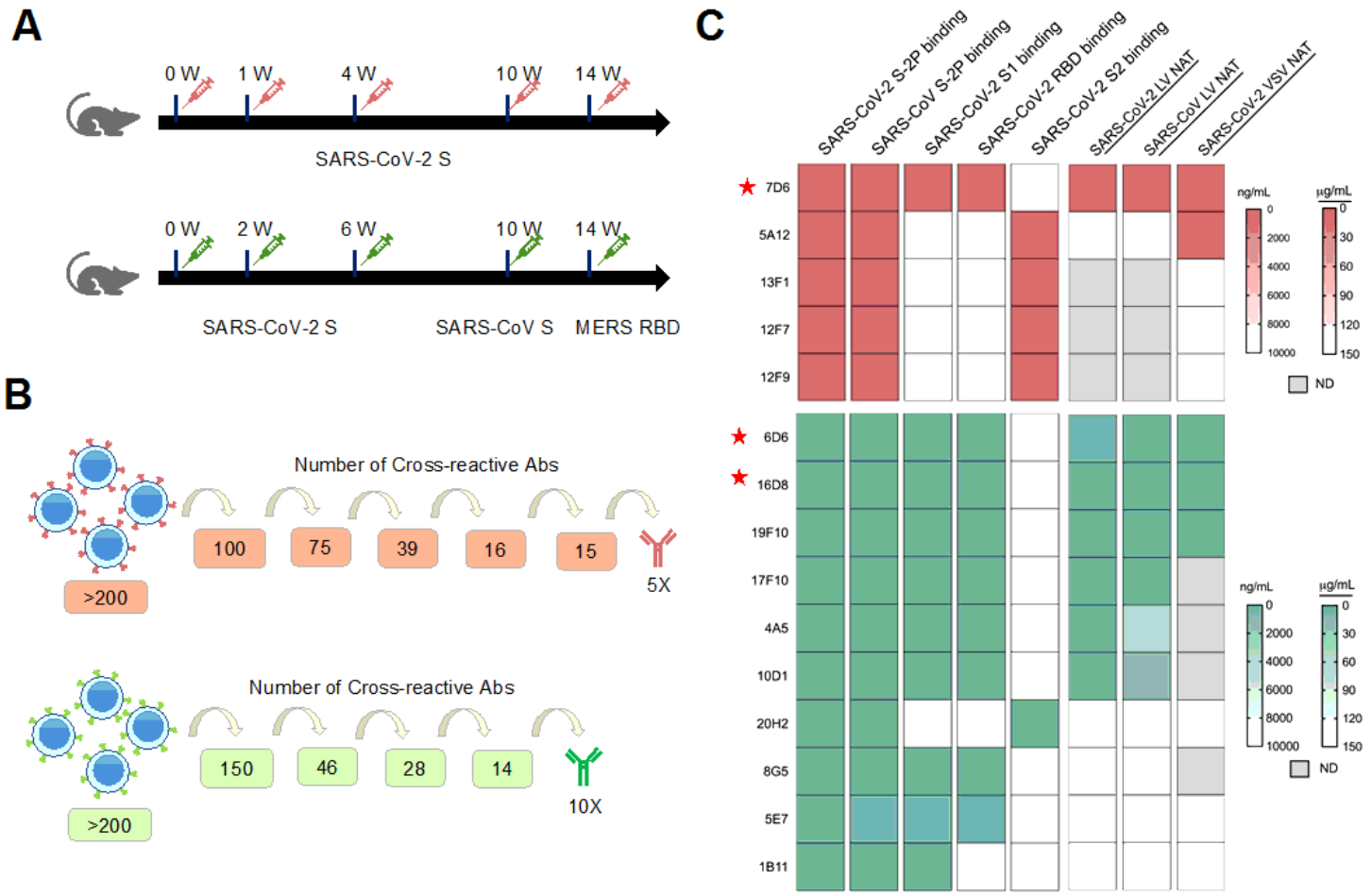

Figure 1

Screening and characterization of SARS-CoV-2 and SARS-CoV cross-reactive monoclonal antibodies. (A) The immunization schemes of two different strategies: immunized with the SARS-CoV-2 spike protein alone (upper) or with a combination of the SARS-CoV-2 and SARS-CoV spike proteins and the MERS-CoV RBD (lower). (B) The number of lead antibodies with cross-activity in each round of screening. (C) Characterization of 5 and 10 monoclonal antibodies obtained by the first and second immunization strategies, respectively. The neutralizing titers (IC50) based on the vesicular stomatitis virus pseudotyping system (VSV NAT) and the lentiviral virus pseudotyping system (LV NAT) were tested. ND means not detected. Asterisks indicate the top 3 monoclonal antibodies with excellent cross-neutralizing potency.

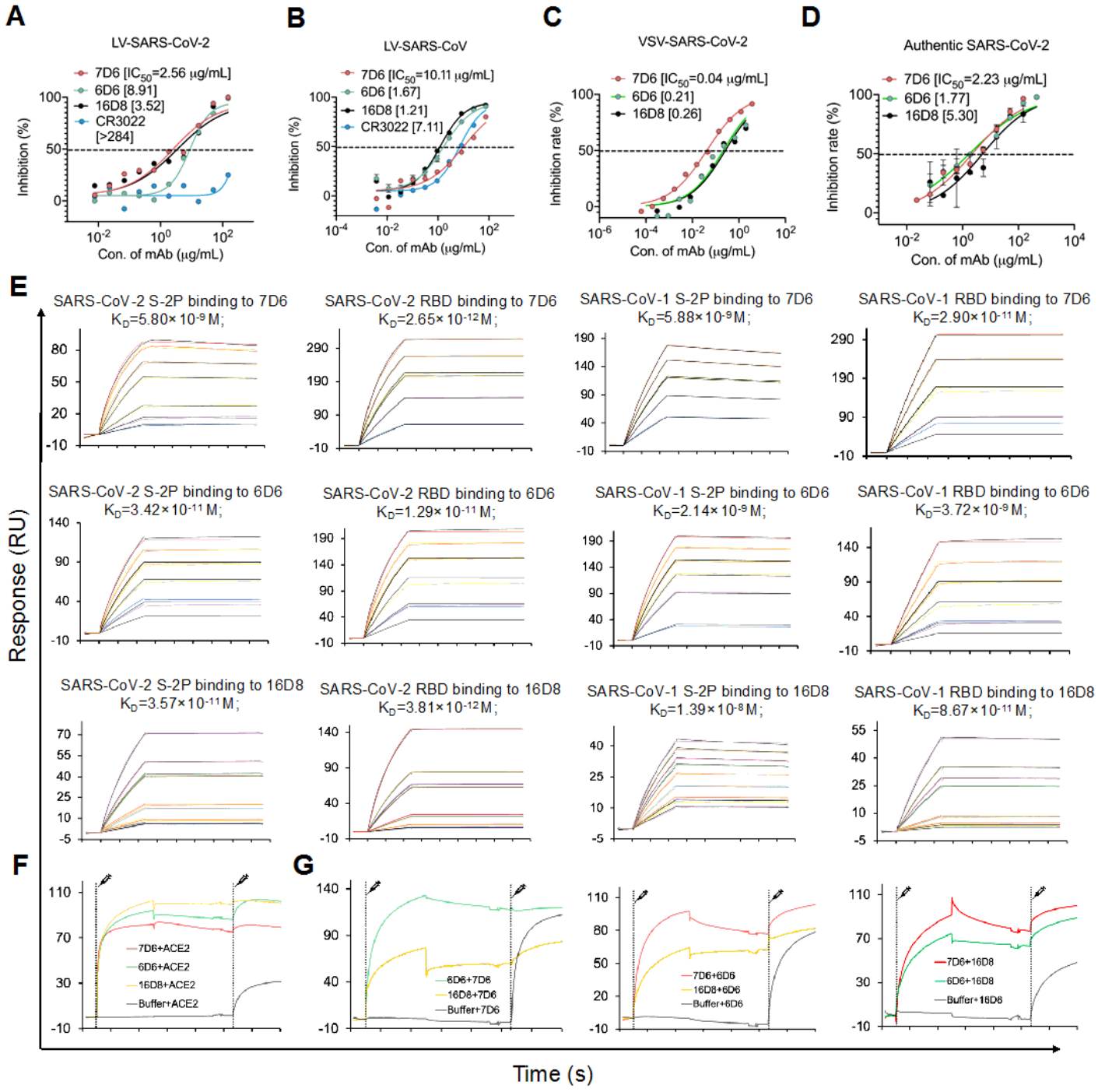

Figure 2

Comprehensive characterization of representative neutralizing mAbs 7D6, 6D6, and 16D8. (A-C) Neutralization of three mAbs by VSV-SARS-CoV-2 (A), LV-SARS-CoV-2 (B) and LV-SARS-CoV (C). (D) Neutralization activities of three mAbs to authentic SARS-CoV-2 virus. (E) SPR kinetics and the affinities of three antibodies to S-2P and RBD proteins of both SARS-CoV-2 and SARS-CoV. (F) SPR-based blocking assays of the three mAbs perturbing the engagement of ACE2 to RBD. (G) Inter-blocking potentials of the three mAbs.

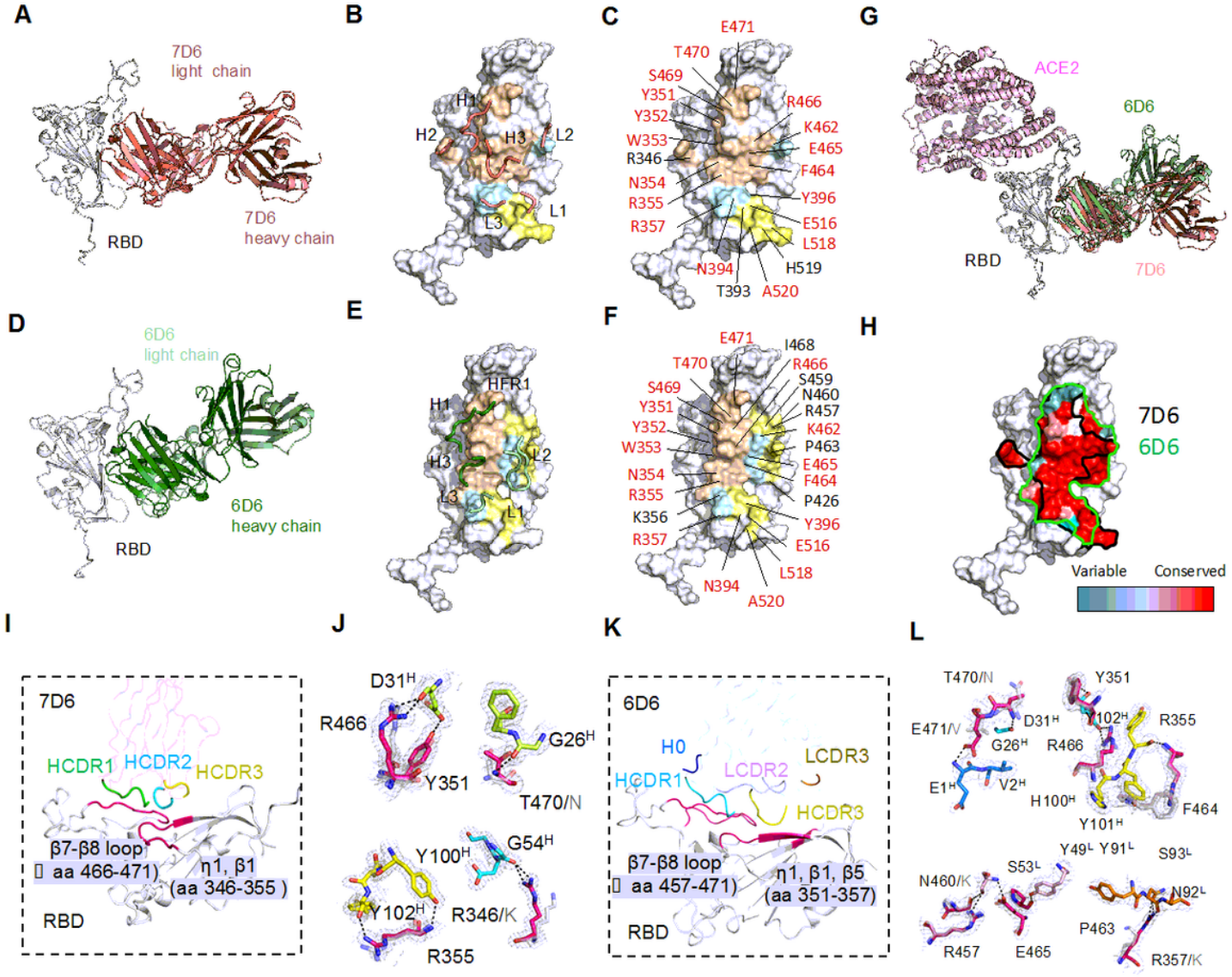

Figure 3

Crystal structures of 7D6 and 6D6 in complex with SARS-CoV-2 RBD. (A, D) Overall structures of 7D6:RBD and 6D6:RBD. (B, E) CDRs of 7D6 (B) and 6D6 (E) involved in the interactions. RBDs and CDRs are shown as surface and cartoon, respectively. The contact surfaces of the heavy (H) and light (L) chains on the RBD are colored in orange and yellow, respectively; residues contacting both the heavy and light chains are colored in cyan. (C, F) Residues on the RBD involved in the interactions with 7D6 (C) and 6D6 (F) are indicated; shared residues are labeled in red. (G) Superimposition of the ACE2:RBD complex (PDB: 6M0J) and our immune-complexes, revealing no competition between ACE2 and the mAbs. (H) Conservation analysis of critical residues in the binding epitopes for 7D6 (outlined in black) and 6D6 (outlined in green). Thirty-four genes encoding for Sarbecovirus spike proteins were selected to calculate conservation. Deeper red indicates more conservation. (I) Interaction between the 7D6 heavy chain variable region and the RBD. The contact region on the RBD is colored purple, and HCDR1-3 are colored in green, cyan, and yellow, respectively. (J) Hydrogen bonds (dashed lines) between 7D6 and RBD. The

electron density (2Fo-Fc) map of all residues is displayed on the contour level of 1σ above the mean value. Conserved residues between SARS-CoV-2 and SARS-CoV are shown in stick mode and in the same color scheme as in (I) for SARS-CoV-2 and in gray for SARS-CoV. (K) Interactions between the 6D6 CDRs and RBD. The contact region on the RBD is colored in purple; H0, HCDR2, HCDR3, LCDR2 and LCDR3 are colored in dark blue, cyan, yellow, pink, and orange, respectively. I, Hydrogen bonds (dashed lines) between 6D6 and RBD.

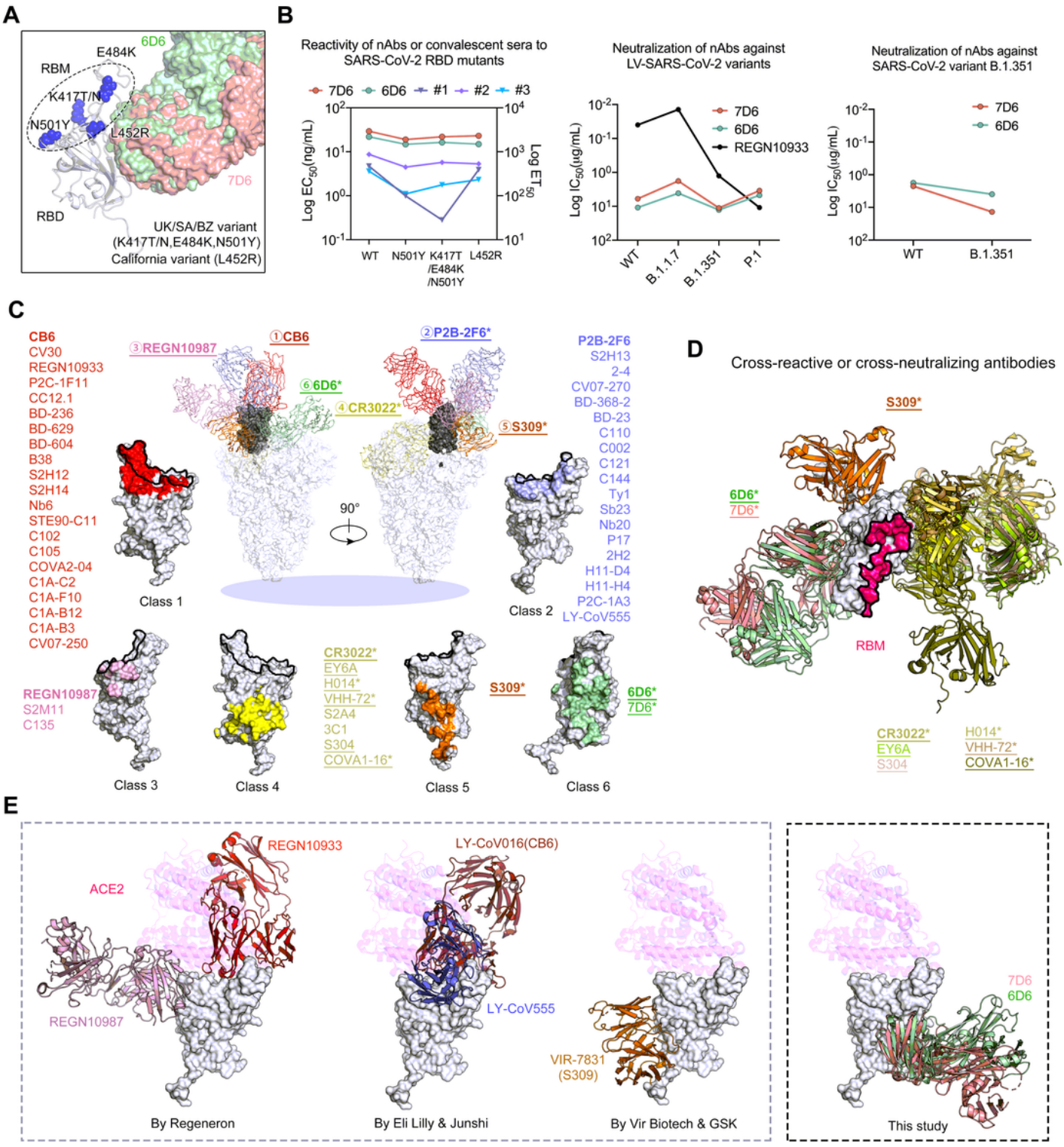

Figure 4

Mutation resistance of 7D6 and 6D6 and comparison of the 7D6/6D6 site with other binding modes of known RBD nAbs. (A) Predominant mutations on the RBD in the SARS-CoV-2 UK, South Africa, Brazil, and California variants. None of these mutations occur within the 7D6/6D6 site. (B) Binding reactivities of 7D6, 6D6 against the RBD mutants and their neutralizing activities against pseudotyped LVs and authentic virus of the major SARS-CoV-2 variant(s). Three convalescent sera and nAb REGE10933 served as control. (C) Superimposed structures of S trimers (shown as gray surface) and six classes of nAb-RBD complexes, the bound RBD were highlighted in dark gray. The epitopes of the six representative nAbs were shown on RBD separately. nAbs belonging to the same class (with similar epitopes or binding modes) are listed in the corresponding color. The underlined antibodies indicate cross-reactive antibodies and the asterisks indicate cross-neutralizing antibodies. (D) Superimposed structures of the Class 4 cross-reactive nAbs (CR3022, Ey6A, S304, H014, VHH-72, and COVA1-16), Class 5 cross-reactive nAb (S309) and Class 6 cross-reactive nAbs (this study; 7D6 and 6D6), showing three different binding orientations. All three classes of nAbs bind epitopes without overlapping the RBM. (E) Comparison of 7D6, 6D6 and antibodies clinically used under EUA. REGN10933 + REGN10987 developed by Regeneron Pharmaceuticals Inc., LY-CoV16 (CB6) + LY-CoV555 from Eli Lilly & Company and Junshi Biosciences Inc., VIR-7831(S309) from Vir Biotechnology and GlaxoSmithKline group of companies (GSK).

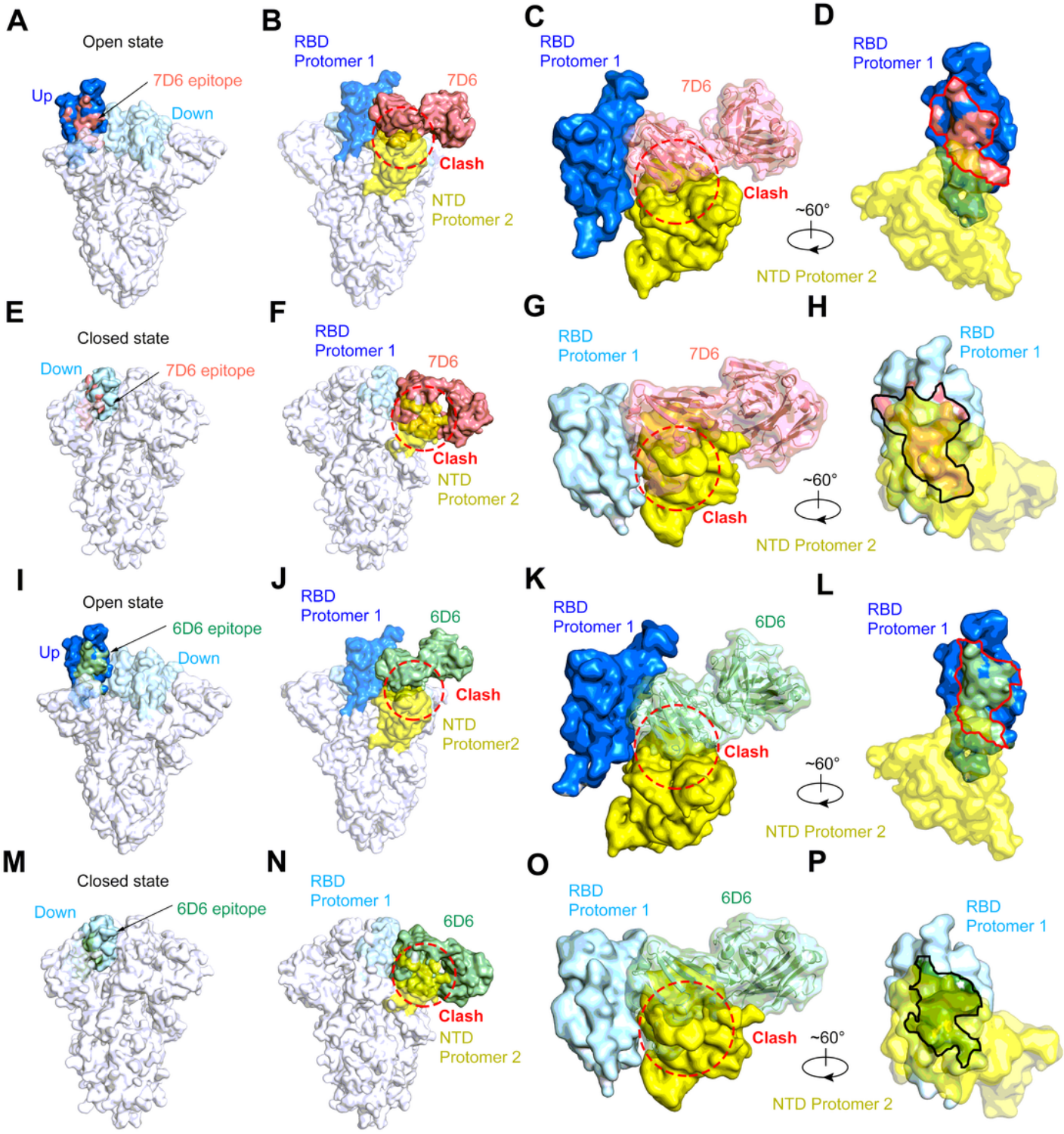

Figure 5

Structural analyses reveal the spatial clash induced by 7D6 and 6D6 binding. (A, E, I, M) Epitope locations of 7D6 and 6D6 on the trimeric spike (PDB: 6zgg) when the RBD is in its open (blue) or closed (cyan) states (PDB:6vxx). 7D6 are colored in salmon and 6D6 in pale green. (B, F, J, N) Superimposition of the 7D6:RBD or 6D6:RBD complex and the open or closed RBD on the trimeric spike. Binding of 7D6 or 6D6 to either the open or closed state of the RBD would cause clashing (indicated by the red dash circles) with

the neighboring NTD. (C, G, K, O) A close-up view of the clash of 7D6 and 6D6 on RBD. (D, H, L, P) Cryptic feature of the epitopes of 7D6 and 6D6 is shown on RBD in surface mode with a neighboring NTD rendered as semi-transparent surface, with close-up views of (C), (F), (J), (N), respectively.

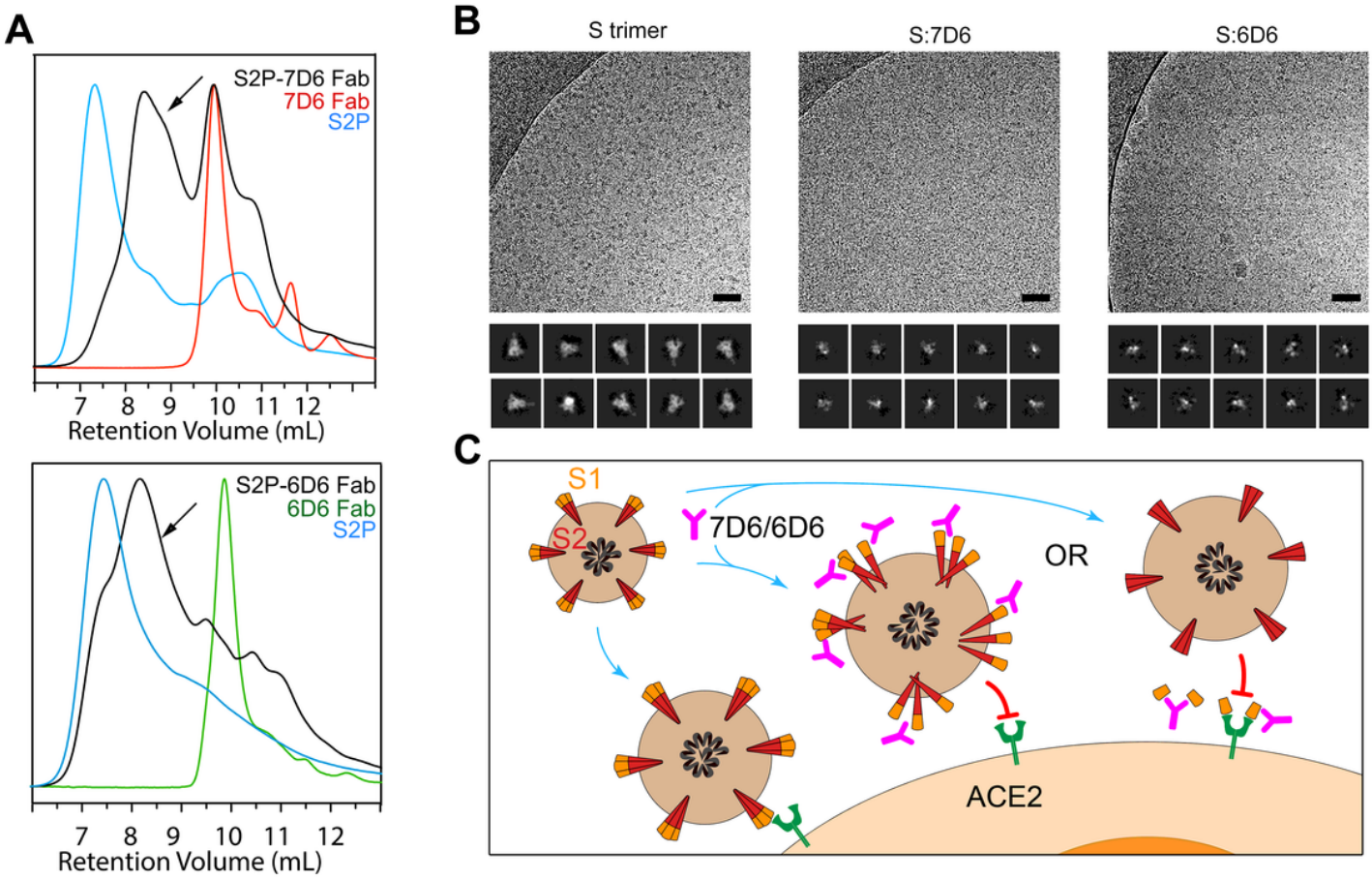

Figure 6

Neutralization mechanism revealed by biochemical and cryo-EM analyses. (A) HPLC profiles of 7D6 and 6D6 binding to the S trimer. The black peak (arrow) indicates depolymerization of the spike. (B) Cryo-EM micrographs (upper) and 2D analysis (lower) of S-2P and its immune-complexes. (C) Two possible mechanisms of 7D6/6D6-mediated neutralization. First, 7D6/6D6 destabilizes SARS-CoV-2 spikes on the virus surface and the disordered spikes lose ability to engage ACE2 receptor. Or second, 7D6/6D6 binding triggers shedding off S1 moieties from S trimers, rendering viruses non-infectious, even though the free 7D6/6D6-bound S1 moieties could still engage ACE2.

Supplementary Files

This is a list of supplementary files associated with this preprint. Click to download.

- SARSCoV2nAbSMJune2ndNC.pdf